Accepted for publication in the Astronomical Journal, 2009 June 12
Preprint typeset using LaTeX style emulateapj v. 2/19/04

THE REDSHIFT SEARCH RECEIVER OBSERVATIONS OF ^{12}CO $J = 1 \rightarrow 0$ IN 29 ULTRALUMINOUS INFRARED GALAXIES

Aeree Chung[1,2], Gopal Narayanan[2], Min S. Yun[2], Mark Heyer[2] and Neal R. Erickson[2]

Accepted for publication in the Astronomical Journal, 2009 June 12

ABSTRACT

We present ^{12}CO $J = 1 \rightarrow 0$ observations of ultraluminous infrared galaxies (ULIRGs) obtained using the Redshift Search Receiver (RSR) on the 14-m telescope of the Five College Radio Astronomy Observatory. The RSR is a novel, dual-beam, dual-polarization receiver equipped with an ultra-wideband spectrometer backend that is being built as a facility receiver for the Large Millimeter Telescope. Our sample consists of 29 ULIRGs in the redshift range of 0.04-0.11, including 10 objects with no prior ^{12}CO measurements. We have detected 27 systems (a detection rate of 93%), including 9 ULIRGs that are detected in CO for the first time. Our study has increased the number of local ULIRGs with CO measurements by $\sim 15\%$. The CO line luminosity $L'_{\rm CO}$, correlates well with far-infrared luminosity L_{FIR}, following the general trend of other local ULIRGs. However, compared to previous surveys we probe deeper into the low CO luminosity end of ULIRG population as a single study by including a number of CO faint objects in the sample. As a result, we find 1) a smoother transition between the ULIRG population and local QSOs in $L_{FIR} - L'_{\rm CO}$ ("star formation efficiency") space, and 2) a broader range of $L_{FIR}/L'_{\rm CO}$ flux ratio ($\sim$60–10^3 $L_\odot$/[K km s^{-1} pc^2]) than previously reported. In our new survey, we also have found a small number of ULIRGs with extreme $L_{FIR}/L'_{\rm CO}$ which had been known to be rare. The mid-IR color and radio-excess of 56 local ULIRGs as a function of FIR-to-CO flux ratio is examined and compared with those of spirals/starburst galaxies and low-z QSOs. In this paper, using a large sample of local ULIRGs we explore the origin of their current power source and potential evolution to QSOs.

Subject headings: galaxies: evolution — galaxies: starburst — ISM: molecules

1. INTRODUCTION

An important discovery from the *IRAS* all-sky survey is a large population of infrared luminous ($L_{IR} \gtrsim 10^{11}$ $L_\odot$) galaxies that are emitting the bulk of their luminosity in the infrared (Sanders & Mirabel 1996). The most extreme objects, so-called "ultraluminous infrared galaxies (ULIRGs)" with $L_{IR} \gtrsim 10^{12}$ $L_\odot$, are the most luminous objects in the local Universe (Solomon et al. 1997). ULIRGs are rare at low redshift ($z \lesssim 0.3$), but their co-moving IR energy density grows rapidly with increasing redshift (LeFloc'h et al. 2005), and galaxies with ULIRG-like luminosity are quite numerous at $z \gtrsim 1$ (Farrah et al. 2003, and references therein). ULIRGs therefore represent an important population for understanding the cosmic star formation history and the cosmic energy budget.

Most ULIRGs appear to be advanced mergers (Sanders et al. 1988a; Farrah et al. 2001) while $\sim$15% of IR luminous systems show characteristics of quasi-stellar objects (QSOs) in their optical spectra (Sanders & Mirabel 1996). Whether the origin of their large IR luminosity is a merger-driven starburst or AGN activity (or both) is still not well established. Their eventual fate is also controversial. In the multi-wavelength study of a flux-limited sample, Sanders et al. (1988a, b) have suggested that ULIRGs hosting an AGN are transition objects that eventually evolve into optically selected QSOs as the AGN light dominates the decaying starburst light.

A common trait found among the ULIRG population is the large molecular gas content ($M_{H_2} \gtrsim 10^{10} M_\odot$), inferred from their observed CO luminosity (Sanders et al. 1991; Young et al. 1995; Solomon et al. 1997), capable of fueling both the bursts of star formation and the AGN activities seen in these systems. Indeed, the correlation between the far-infrared luminosity L_{FIR} and the CO line luminosity $L'_{\rm CO}$ of ULIRGs forms a continuous track with those of QSOs in the Local Universe (Riechers et al. 2006, and references therein), which is supportive of the proposed ULIRG-QSO evolution scenario. QSOs with $L_{IR} > 10^{12}$ $L_\odot$ however are rare in the Local Universe, implying that ULIRGs are not simply a stage of transition to QSOs (Farrah et al. 2001; Yun et al. 2004) or that the transition may occur quite rapidly (Yun et al. 2004).

Considering the rich history of multi-wavelength investigations of the ULIRG phenomenon and their importance as the local analogs to the luminous dusty galaxies found in the early universe (so-called "submillimeter galaxies (SMGs)"; see review by Blain et al. 2002), it is surprising that the total number of published CO measurements for ULIRGs is limited to only $\sim$50 or so, primarily from the surveys conducted by Sanders et al. (1991) and Solomon et al. (1997)[3], and by Mirabel et al. (1990) for southern objects. There have been also some CO studies of individual ULIRGs in the Local Universe ($z \lesssim 0.3$, e.g. Combes et al. 2006), although these do not contribute to the total number statistics by large.

[1] Jansky Fellow, National Radio Astronomy Observatory; email: achung@aoc.nrao.edu
[2] Department of Astronomy, University of Massachusetts, 710 North Pleasant Street, Amherst, MA 01003, USA; emails: gopal@astro.umass.edu, myun@astro.umass.edu, heyer@astro.umass.edu, neal@astro.umass.edu

[3] More recent ULIRG surveys of the higher J CO transitions (Yao et al. 2003; Narayan et al. 2005) have targeted mostly the same sample.

This limited information on CO emission and molecular gas content reflects both the rarity of ULIRGs in the local volume and the challenge of detecting CO emission from galaxies even at these modest distances. It raises a real concern that the existing CO data may be too small to characterize the molecular gas properties of the ULIRG population with sufficient statistics. The existing CO data may also reflect strong biases in the sample selection and/or the survey strategies adopted by these earlier studies. In comparison, the total number of CO measurements available for the $z > 1$ SMGs is >30 systems (see review by Solomon & vanden Bout 2005), which is generally considered too few to draw any broad conclusions about the molecular gas content and properties of the SMG population.

In order to address these issues, we have conducted a new CO survey of 29 ULIRGs in the redshift range $z \approx 0.04$-0.11 using the sensitive, ultra-wideband spectrometer system called the Redshift Search Receiver (RSR) on the Five College Radio Astronomy Observatory (FCRAO) 14-m telescope. The broad spectral coverage of the RSR enables a CO line detection even in cases where the reported optical redshifts might have been significantly in error. Our sample is comparable in size to the largest previous CO surveys of ULIRG population (e.g. Solomon et al. 1997), but probes deeper into the CO luminosity by including more CO faint objects in the sample as a single study. Our sensitivity allowed us to detect a number of sources with the comparable line intensity as the faintest ULIRGs in CO that have been known to date (e.g. IRAS 08572+3915 by Solomon et al. 1997 or IRAS 10173+0828 by Sanders et al. 1991).

This paper is organized in the following order. In §2 we describe our sample selection criteria and the properties of the sample. In §3 we describe the observations and data reduction. In §4 we present the results and discuss the data quality. In §5 the origin of IR emission and the evolution of the local ULIRGs are discussed. Finally in §6 we summarize our findings. We assume a standard ΛCDM cosmology with H_0 =71 km s^{-1} Mpc^{-1}, Ω_M =0.27, and Ω_Λ =0.73 (Spergel et al. 2003) throughout the paper.

2. SAMPLE

Our sample is constructed primarily from the 1 Jy ULIRG[4] sample, which consists of 118 sources identified from the IRAS Faint Source Catalog (Moshir et al. 1990) with $S_{60\mu} > 1$ Jy, $\delta > -40°$, and $|b| > 30°$ (Kim & Sanders 1998). All 18 ULIRGs in the 1 Jy Sample whose ^{12}CO $J = 1 \rightarrow 0$ line falls within the frequency range of $\nu_{\rm obs} \approx 104$-$111$ GHz (z =0.043-0.11, see §3) were selected as the primary sample. In addition, we have selected four targets from the 2 Jy sample of Murphy et al. (2001) with $S_{60\mu} > 1.94$ Jy, $\delta > -35°$, and $|b| > 5°$. Lastly, in order to provide comparison with our observations (§ 4.2), 20 ULIRGs with previous CO measurements were added from Mirabel et al. (1990), Sanders et al. (1991), Solomon et al. (1997), and Gao & Solomon (1999). Those ULIRGs were all previously detected except for IRAS 20414−1651 (Mirabel et al. 1990). These include 13 sources which overlap with the sample from Kim & Sanders (1998) or Murphy et al. (2001), or both, yielding the total number of our sample 29. General properties of the 29 ULIRGs are summarized in Table 1.

The optical Digitized Sky Survey plate images of all 29 ULIRGs and the color images of 12 available ULIRGs from the Sloan Digital Sky Survey data archive are presented in Figure 1 and 2. As shown in the optical images, morphological peculiarities are quite common in ULIRGs. Many galaxies show faint stellar tails (e.g. IRAS 12112+0305), rings (IRAS 15250+3609), or extended/asymmetric low surface brightness disks (e.g. IRAS 10565+2448). More than 75% of the sample are classified as HII, LINER or a starburst systems. Three objects IRAS 05189−2524, IRAS 08572+3915, and IRAS 12540+5708 (Mrk 231) have previously been identified as "*warm*" ULIRGs with $f_{25}/f_{60} > 0.2$ by Sanders et al. (1988b), and another three (IRAS 14394+5332, IRAS 15130−1958, and IRAS 15250+3609) have warm IR color ($0.18 \lesssim f_{25}/f_{60} \lesssim 0.2$), which is indicative of active galactic nuclei (AGN; de Grijp et al. 1985). In addition, IRAS 00057+4021 and IRAS 15462−0450 are classified as Seyfert type 2 and 1, respectively, and likely harbor an AGN.

Our study is one of the most systemic and deepest CO surveys of a fairly large sample of ULIRGs to date, including 9 objects with no prior CO measurments and one which was observed but not detected.

3. OBSERVATIONS AND DATA REDUCTION

3.1. *Observations with the RSR on the FCRAO 14-m Telescope*

The observations presented here were conducted using the Five College Radio Astronomy Observatory (FCRAO) 14-m telescope between March and May in 2007 and in 2008 May. The FCRAO 14-m telescope is a radome-enclosed single-dish millimeter telescope, located on Prescott peninsula within the Quabbin Reservoir, Massachusetts. The spectra were taken using the Redshift Search Receiver (RSR). The RSR is a sensitive, ultra-wideband spectrometer that is being built at the University of Massachusetts as one of the facility instruments for the 50-m diameter Large Millimeter Telescope (LMT).

The RSR consists of a frontend receiver which uses a novel construction for a millimeter wavelength system and a set of wide-band analog auto-correlation spectrometers. There are four receivers each covering 74-111 GHz instantaneously in a dual-beam, dual-polarized system. The input includes a novel electrical beam switch which operates at 1 kilohertz (kHz) to overcome the 1/f noise originating within the frontend amplifiers as well as atmospheric noise to ensure excellent baseline stability. The frontend uses MMIC (monolithic microwave integrated circuit) amplifiers and two very wideband mixers to convert each receiver band to two intermediate frequency (IF) channels. After further conversion, the IF signal passes into a spectrometer based on analog autocorrelation. Sets of tapped delay lines sample and multiply the signal with progressive delays to generate a spectrum with 31 MHz resolution. Six spectrometers, each covering 6.5 GHz bandwidth, are used with each pixel. The entire 36 GHz of bandwidth of each pixel is handled by six boards, each having 256 lags (in all 1536 lags per

[4] The conventional definition of an ultraluminous infrared galaxy is a galaxy with rest-frame 1-1000 μm luminosity of $L_{IR} \geq 10^{12}\ L_\odot$ (see Sanders & Mirabel 1996).

TABLE 1
General Properties of the Sample of 29 ULIRGs[a]

IRAS name	Other Name	α_{2000} ($hhmmss.s$)	δ_{2000} (° ′ ″)	cz (km s^{-1})	m_B (mag)	D_{opt} (″)	$t_{\rm int}$ (hrs)	rms (mK)	Morphology	Reference[b]
00057+4021	PGC 000626	00 08 20.5	40 37 57	13389	16.78	0.46	2.9	0.50	Sy2	S97
05083+7936	VII Zw 031	05 16 46.4	79 40 13	16090	15.80	...	1.9	0.65	HII	S97
05189−2524		05 21 01.4	-25 21 46	12760	15.40	0.46	3.6	0.65	Pec Sy2	M90, S91 [KS98]
08572+3915		09 00 25.0	39 03 54	17493	14.92	...	8.2	0.31	LINER; Sy2	S97, GS99 [KS98, M01]
09111−1007	LEDA 153577	09 13 38.8	-10 19 20	16231	16.11	0.70	2.5	0.53	HII Sy2	M90 [M01]
10035+4852	PGC 029385	10 06 46.2	48 37 46	19430	15.70	0.80	1.5	0.57	Sbrst	S97 [KS98, M01]
10173+0828	PGC 030202	10 20 00.2	08 13 34	14716	16.90	0.44	3.7	0.38	Megamaser	S91
10190+1322	LEDA 090120	10 21 42.5	13 06 54	22955	17.51	0.30	5.7	0.31	HII	S97 [KS98, M01]
10494+4424	LEDA 090133	10 52 23.2	44 08 48	27599	17.40	0.34	10.8	0.25	LINER	S97 [KS98, M01]
10565+2448	PGC 033083	10 59 18.1	24 32 34	12921	15.70	0.40	1.4	0.60	LINER; HII	S97
11095−0238		11 12 03.4	-02 54 22	31968	17.45	0.17	6.3	0.38	Merger LINER	[KS98, M01]
12112+0305		12 13 46.0	02 48 38	21980	16.90	0.50	1.2	0.63	LINER; HII	S91 [KS98, M01]
12540+5708	Mrk 231	12 56 14.2	56 52 25	12642	14.41	1.30	2.5	0.55	SA(rs)c? pec Sy1	S91, S97 [KS98]
13539+2920	LEDA 84081	13 56 10.0	29 05 35	32513	16.90	0.40	7.0	0.27	HII:	[KS98]
14348−1447	PGC 052270	14 37 38.3	-15 00 22	24802	16.58	0.60	3.8	0.82	Merger: LINER	M90, S91 [KS98, M01]
14394+5332	LEDA 084264	14 41 04.4	53 20 09	31341	17.20	0.21	4.2	0.36	Sy2	[KS98, M01]
15130−1958	LEDA 090203	15 15 55.2	-20 09 17	32792	17.10	...	2.0	0.73	Sy2	[KS98]
15250+3609	PGC 055114	15 26 59.4	35 58 38	16535	16.20	0.44	5.2	0.38	Ring; LINER	[M01]
15462−0450	LEDA 090222	15 48 56.8	-04 59 34	29917	16.40	...	3.4	0.46	Sy1	[KS98, M01]
16487+5447	LEDA 090261	16 49 47.0	54 42 34	31106	16.50	...	6.1	0.31	Sbrst LINER	GS99 [KS98, M01]
17028+5817	LEDA 090270	17 03 41.9	58 13 44	31805	17.12	...	3.8	0.50	E;LINER;Sbrst HII	[KS98, M01]
17132+5313	PGC 059896	17 14 20.0	53 10 30	15270	...	...	2.5	0.46	HII	S91, GS99
17208−0014	PGC 060189	17 23 21.9	-00 17 01	12834	15.10	0.40	2.5	0.67	Sbrst HII	M90, S97
18470+3233		18 48 53.8	32 37 28	23517	16.00	0.10	4.0	0.42	Pair HII	[M01]
19297−0406		19 32 21.2	-03 59 56	25701	16.00	0.22	5.7	0.37	Merger HII:	S97
20414−1651		20 44 18.2	-16 40 16	26107	17.10	...	7.8	0.34	LINER; HII Sbrst	M90 [KS98, M01]
22491−1808	PGC 069877	22 51 49.0	-17 52 23	23312	16.15	0.30	5.1	0.32	Merger; HII	M90, S91 [KS98, M01]
23327+2913		23 35 11.9	29 30 00	32078	16.80	...	4.3	0.36	LINER	[KS98, M01]
23365+3604	LEDA 090429	23 39 01.3	36 21 09	19331	16.30	0.46	4.3	0.45	SBa? pec LINER	S97 [M01]

[a]These data have been compiled from the NASA/IPAC Extragalactic Database (NED) which is operated by the Jet Propulsion Laboratory, California Institute of Technology, under contract with the National Aeronautics and Space Administration.
[b]References for previous CO measurements: M90-Mirabel et al. (1990); S91-Sanders et al. (1991); S97-Solomon et al. (1997); GS99-Gao & Solomon (1999) [References for the optical studies: KS98-Kim & Sanders (1998)'s 1Jy sample; M01-Murphy et al. (2001)'s 2 Jy sample]

pixel). Occasionally, a few of the lags develop problems, which are flagged and blanked out before converting to the frequency domain. However, less than 1% of all lags had such problems, and most of these faulty lags have since then been fixed in the spectrometer when the receiver was taken off the telescope More details of the RSR and the LMT can be found in Erickson et al. (2007).

During the observing season in 2007, all four frontend pixels (receivers) were available while only 4 of the 24 backend spectrometers had been fabricated. This yielded a set of 4-frontend pixels × 1-backend spectrometer with a bandwidth range of 104-111 GHz (1st LO could be tuned), and this spectral coverage ultimately limited the redshift range in our sample selection. In 2008, 12 spectrometers became available, and we had a set of 4-pixels × 3-spectrometers with an instantaneous frequency coverage of 92-111 GHz. Therefore some of our new spectra cover a much larger spectral (redshift) range, but we focus on the analysis of only the ^{12}CO $J = 1 \rightarrow 0$ transition in this paper.

We integrated between 1 and 11 hours (Table 1) on each source depending on the weather conditions and the peak of the CO intensity. The system temperature during the run varied from 165 to 380 K with a typical value of $T_{sys} \sim 200$ K in both years. For calibration, normally we obtained one 5-min scan on the reference sky every three consecutive 5-min scans on the target. When the weather was bad ($T_{sys} \gtrsim 400$ K), we did calibration every other scan although most scans obtained under those weather conditions were thrown away in the final co-addition. As a result, we achieved a typical rms sensitivity of $\sigma \lesssim 0.5$-0.6 mK in T_A^* (corrected antenna temperature for the atmosphere absorption and spillover losses). We checked the pointing and the focus using planets every 2 to 3 hours. The antenna gain was monitored by measuring the intensity of planets. An average gain factor of G= 45 Jy K^{-1} is adopted (in T_A^* scale).

3.2. *Data Reduction Using SPAPY*

The RSR data have been reduced using the `SPAPY` (`SPA` + `PYthon`). `SPAPY` is a data reduction software that has been developed by G. Narayanan mainly for the RSR data reduction. For each galaxy, the final spectrum is constructed using the following procedure. First a set of scans of different pixels were individually inspected in

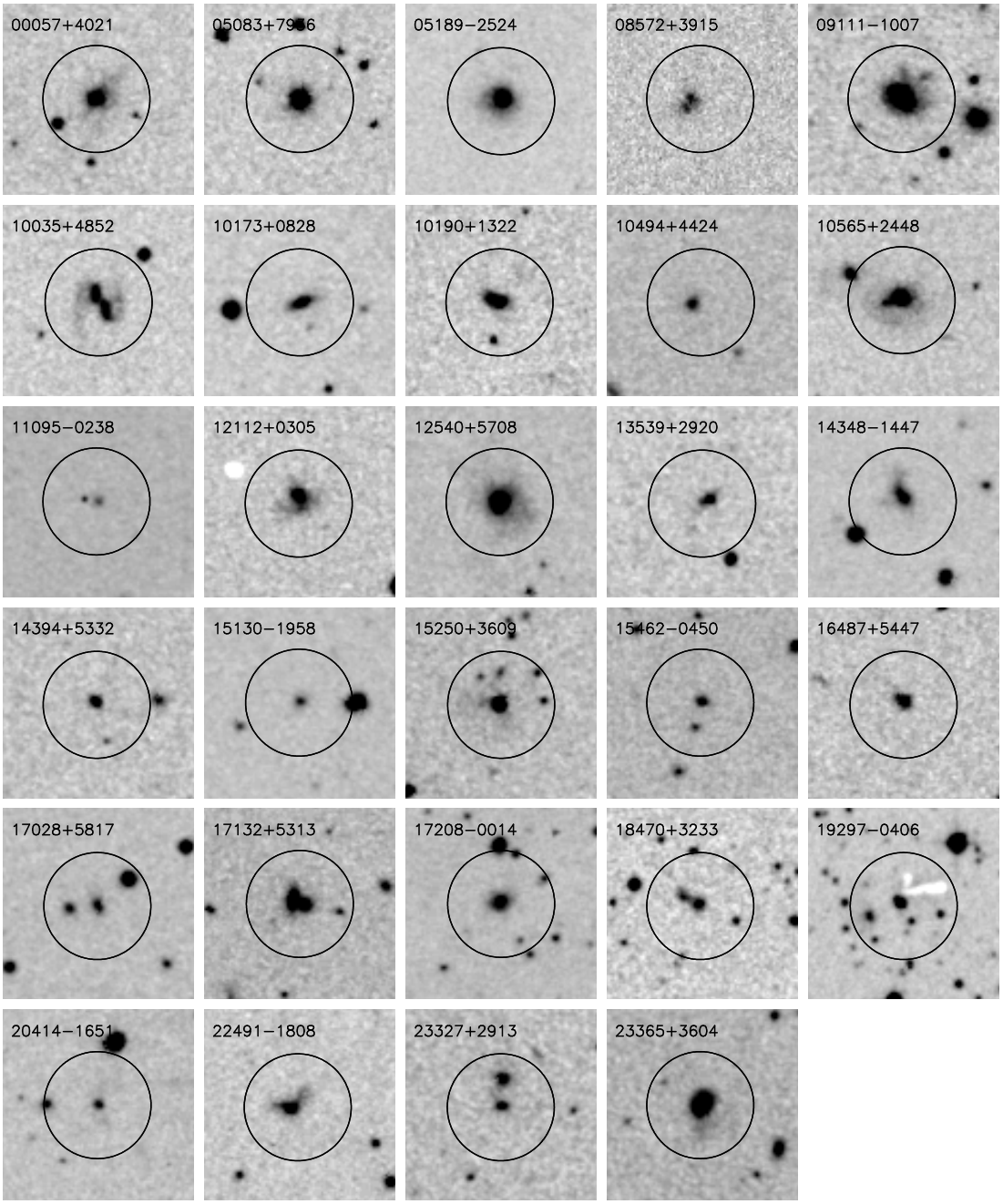

FIG. 1.— Optical images from the 2nd Digitized Sky Survey (DSS2) of the sample of 29 local (z = 0.043-0.11) ULIRGs. Each field ($1.5' \times 1.5'$) is centered on $(\alpha, \delta)_{2000}$ as shown in Table 1. The *IRAS* catalog number is indicated on the top of each panel. A circle of 50″ (≈beamsize of 14m at 3mm) is shown in solid line.

order to exclude data obtained under bad weather conditions or with serious instrumental noise. Then continuum channels are selected that exclude channels with CO line emission and the end channels affected by the bandpass roll-off. A linear baseline is fitted over these continuum channels to calculate the rms noise of each scan. A set of scans for each object are summed weighted by the rms noise. Lastly, a baseline is removed from the combined spectrum, using the same frequency range where we measure the rms of individual scans. For most galaxies, a linear baseline has been fitted while a second order fit has been adopted in some cases, especially for galaxies with low signal-to-noise. The second order fit barely changes the rms over the entire band ($\lesssim 5\%$) but it helps to bring out weak line features by modifying the local baseline structure around the CO line. The measured rms value of the fully processed spectrum for each galaxy is listed in Table 1.

In Figure 3 (a)-(d), the coadded spectra of 29 ULIRGs are shown, which have been divided into four groups depending on the signal-to-noise. On the left-side of each object, the full band spectrum, the full band spectrum excluding noisy end channels is presented in the same T_A^* scale. Twenty seven objects in group (a), (b), and (c) are

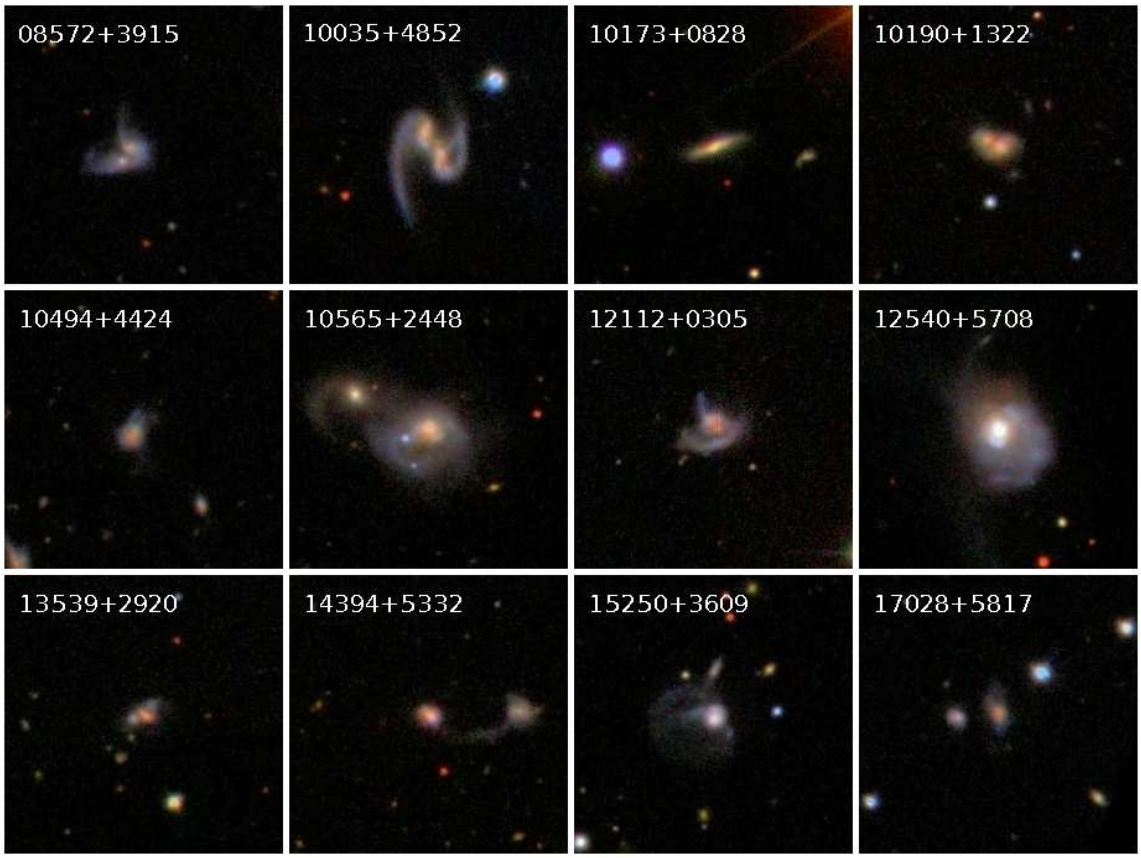

FIG. 2.— The optical color images from the Sloan Digital Sky Survey (SDSS, `http://www.sdss.org/`) of 12 ULIRGs. The size of each field is the same as Figure 1.

qualified as detection by revealing a $> 3\sigma$ feature within a few 100 km s^{-1} around the inferred CO frequency from the optical redshift, which are marked with dotted lines in the full band spectra in Figure 3 (a)-(d). Except for 2 ULIRGs in group (d) which fail our definition of detection, the rest 27 have been classified from (a) to (c) based on the following criteria:

(a) *Bright* or *Intermediate*: In seven ULIRGs with S/N> 7 (bright), and in another seven objects with 3.5<S/N< 7, $W_{\rm CO} > 250$ km s^{-1} and the peak flux density $F_{\rm CO}^{\rm peak} > 1.5$ mK (intermediate), the lines can be picked out without any difficulty.

(b) *Faint* or *Narrow*: Among eight ULIRGs with 3.5<S/N<5.5, ve objects with $F_{\rm CO}^{\rm peak} \lesssim 1.5$ mK but $W_{\rm CO}$ >200 km s^{-1} (faint), and three objects with $W_{\rm CO}$ <200 km s^{-1} yet $F_{\rm CO}^{\rm peak} \gtrsim 1.4$ mK (narrow) still show well dened line features.

(c) *Marginal*: There are five ULIRGs that still meet our detection criteria but the lines are not as prominent as the other two groups (1< $F_{\rm CO}^{\rm peak} < 1.2$ mK). There could be some confusion with nearby noise structure as indicated by the error in $W_{\rm CO}$ of $\gtrsim 40\%$.

As seen in the full band spectra, the baselines are fairly flat throughout the entire frequency coverage with well behaved noise. This is also demonstrated in Figure 4 where the rms from the full band (Table 1) are compared with the local rms which were measured using the continuum channels within $\sim 1-2$ GHz range around the CO line. In most cases, the rms are found along the equivalent line with $\lesssim 10\%$ of variation.

It should be noted that such flat baselines over such wide bandwidths have hitherto not been reported for millimeter wave receivers, and is a result of the innovative design of the RSR. The flat baseline of the RSR with well behaved noise will be particularly important for a blind line search of galaxies with no previous redshift measurement, and hence this demonstration has been one of our goals in this study. These characteristics of the RSR also allowed us to integrate down to detect fainter lines, yielding 93% of the detection rate including 5 marginal detections. The two non detections might be due to the insufficient band coverage. In particular, Gao & Solomon (1999) reported the CO luminosity of IRAS 16487+5447 which is almost three times larger than our upper limit based on the CO line intensity upper limit (3×rms×250 km s^{-1}, § 4.1). However, our baseline fit has successfully brought up the line close to the band edge even in some cases with marginal signal-to-noise. Therefore we suggest that those two galaxies may contain molecular gas of low flux density with a huge line width (> 500 km s^{-1}) as found in some extreme cases like IRAS F11180+1623 by Dinh-V-Trung et al. (2001).

4. RESULTS

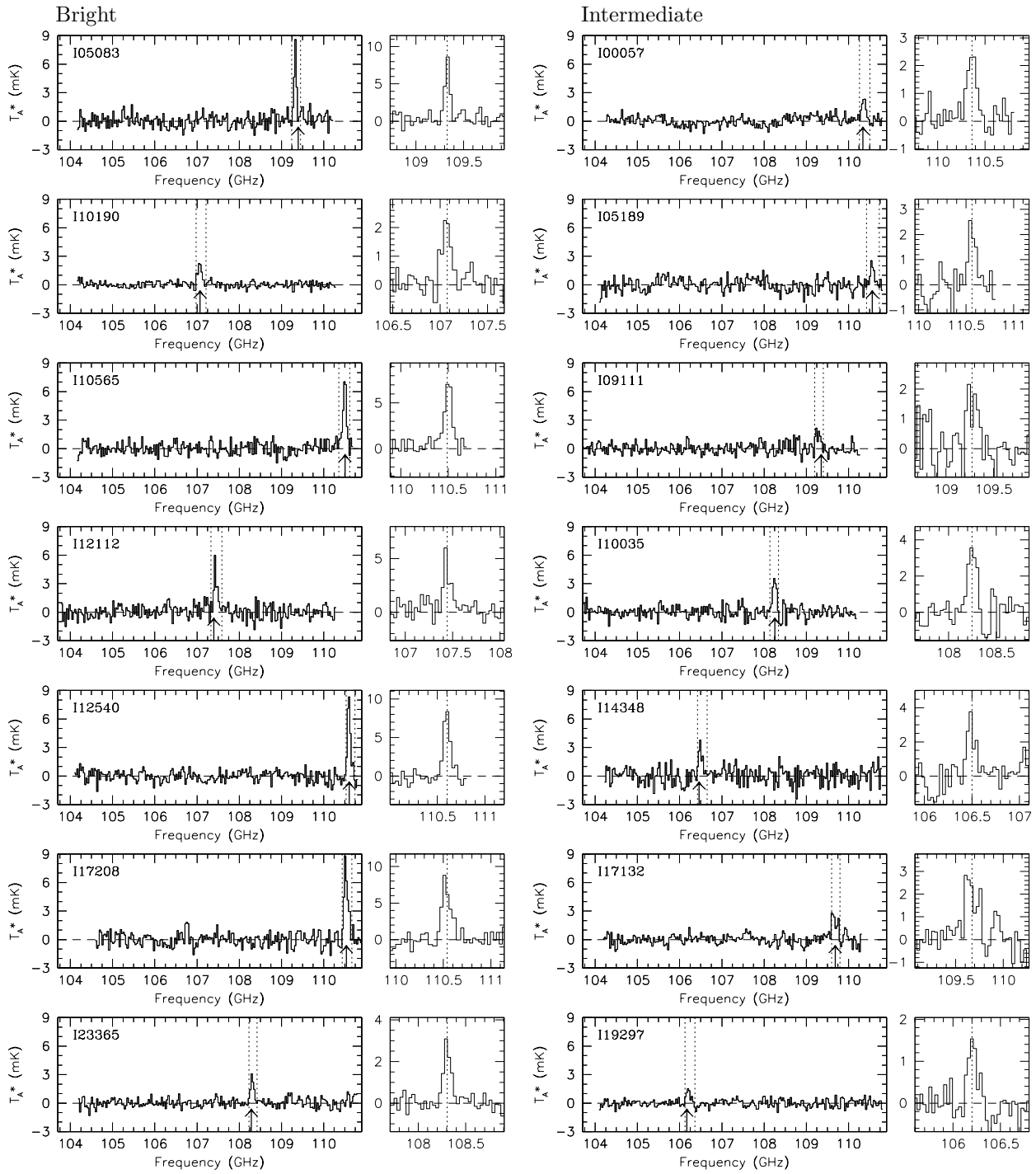

FIG. 3.— (a) The RSR spectra of 14 ULIRGs with a high (left column) to intermediate (right column) CO strength. The quantitative descriptions for the classication are given in §4.2. On the left side of each ob ject, the full abdn spectrum is shown except for a few noisy channels at the edge. On the right-hand side, each spectrum is zoomed-in around the CO emission. The full-band spectra with the frequency range of 103.7-110.9 GHz are shown in the same T_A (antenna temperature corrected for the atmosphere absorption and spillover losses) scale for all galaxies. The dotted lines in each full-band spectrum represent the frequency range used to measure the CO intensity and derive the CO line width. The upper arrow indicates the estimated CO frequency from the optical redshift. The zoom-in spectra of 1.2 GHz (∼3100 km s^{-1}) width centered on the CO frequency are scaled down with the peak of the CO emission. The dotted line in the zoom-in spectrum represents the centroid CO frequency.

4.1. *Measuring the CO Quantities*

Integrated intensity ($I_{\rm CO}$), center frequency (ν_{CO}) and CO line width ($W_{\rm CO}$) are determined from the final reduced spectra. The integrated line intensity in K kms^{-1} is calculated by summing the flux density of the line channels,

$$I_{\rm CO} = \sum_{line} F_{line} \frac{\Delta\nu}{\nu_{line}} c \ \ K\ km\ s^{-1} \qquad (1)$$

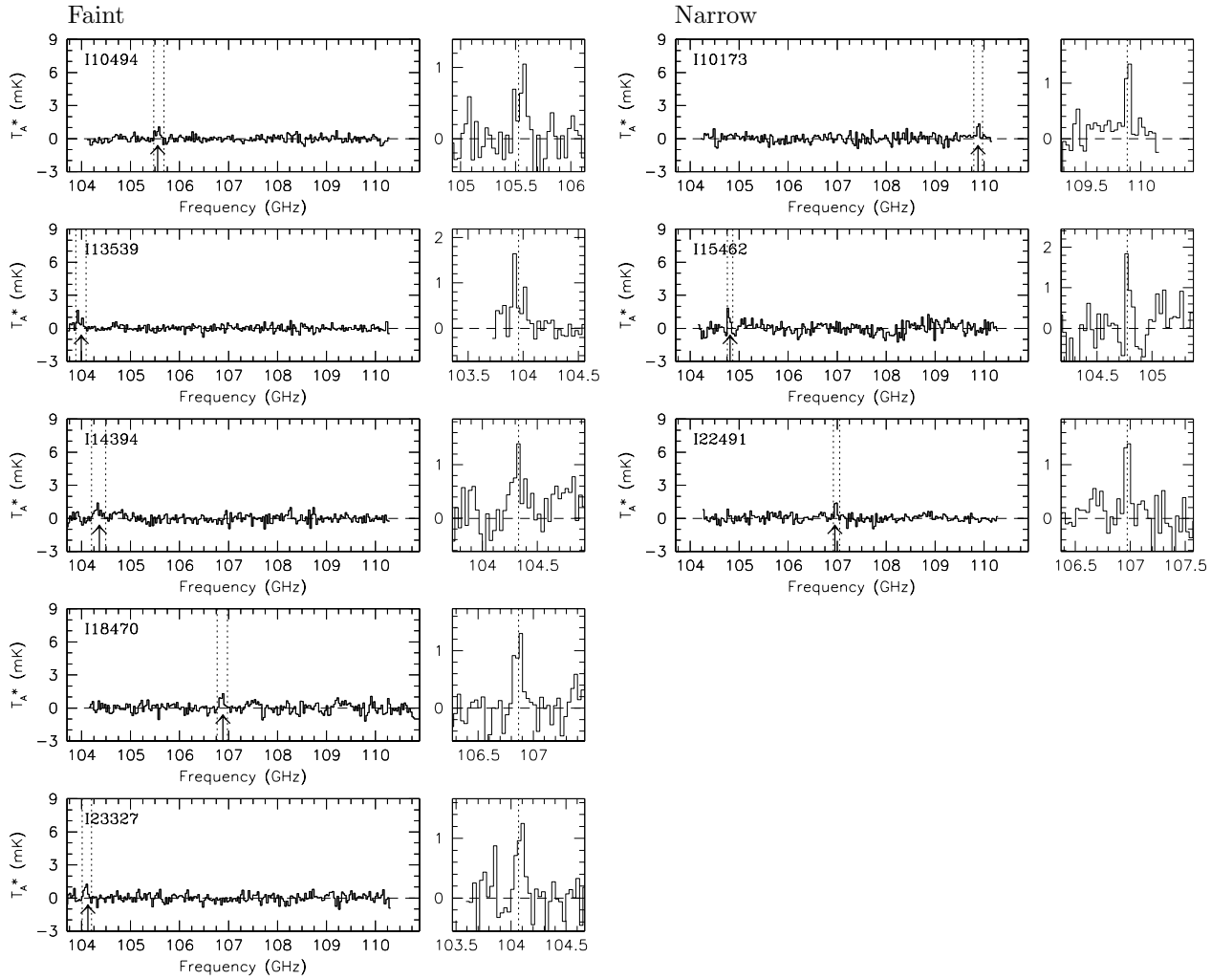

FIG. 3.— (b) The RSR spectra of 5 ULIRGs that are faint in CO (left column) and 3 ULIRGs that are faint and narrow (right column). See the caption of Figure 3-(a) for more details.

where F_{line} is flux density in K at each line channel, $\Delta\nu$ is the channel width (0.031 GHz for the RSR), ν_{line} is the central frequency of each spectral channel in GHz, and c is the speed of light in km s^{-1}. The central frequency, $\nu_{\rm CO}$ has been calculated as a first moment of the spectrum in the same frequency range used to measure $I_{\rm CO}$. The line width, $W_{\rm CO}$, is calculated as $I_{\rm CO}/F_{\rm peak}$. For the two non-detections, the quoted 3σ upper-limits are estimated assuming a line width of 250 km s^{-1} (cf. the mean line width $W_{\rm CO}$ of the 27 CO detected galaxies$\approx$ 264 $\pm$ 60). The rms noise locally measured around the CO line ($<$ 2 GHz, Table 2) has been adopted to calculate the upper limits. The measured CO quantities are summarized in Table 2.

4.2. *Comparisons with Previous Measurements*

Among the prior CO studies of LIRGs/ULIRGs, Solomon et al. (1997) collected coherent CO data using the IRAM 30m telescope of 37 ULIRGs and is the most comparable with our study. A comparison of our $I_{\rm CO}$ of 11 ULIRGs which were also observed by Solomon et al. (1997) is shown in Figure 5. Gain factors G =45 and 4.5 Jy K^{-1} in T_A^* and T_{mb} scale are adopted for the 14m and 30m telescope, respectively. In Table 3, $I_{\rm CO}$ from the 14m telescope is given in Jy km s^{-1}. As shown in Figure 5, most of the objects are within their 1σ measurement uncertainty from the $I_{\rm CO,30m} = I_{\rm CO,14m}$ line and $I_{\rm CO}$ from the two telescopes are overall in good agreement.

In Figure 6, we directly compare the 14m spectra with those from the 30m for four objects with a range of signal-to-noise: one CO bright object (I12540, also known as Mrk 231), one with intermediate brightness (I00057), one CO faint object (I10494), and one with a marginal detection (I08572). As shown on the left side of the figure, the 14m spectra are generally in good agreement in spite of the low spectral resolution ($\sim$90 km s^{-1} vs. 24 or 48 km s^{-1} for 30m). There may be some confusion in the cases of marginal detections although the discrepancy in the total flux is expected not more than 40% inferred from the comparison of I08572. Lastly, the redshifts determined from our CO spectra (Table 3) are consistent with optical redshifts for the 27 detected sources, with $\Delta < V_{CO} - V_{opt} >= 121 \pm 93$ km s^{-1}.

A comparison of the distribution of CO luminosities for our survey sample and those in the same redshift

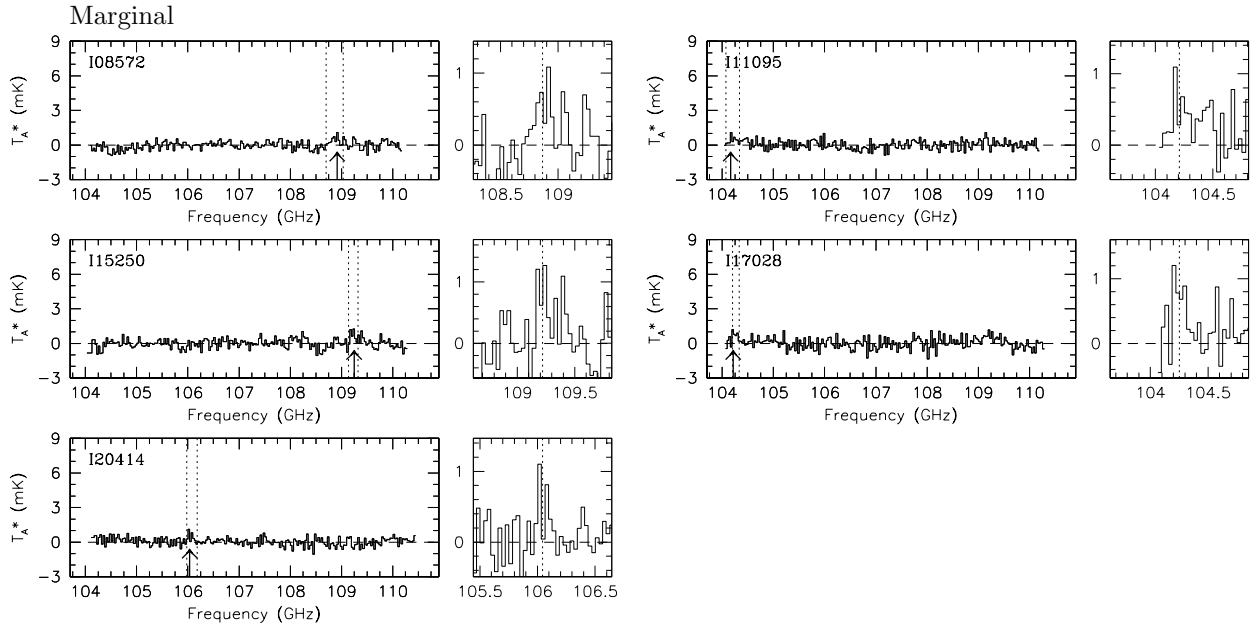

FIG. 3.— (c) The RSR spectra of 5 ULIRGs of marginal detections. See the caption of Figure 3-(a) and §3.2 for further details.

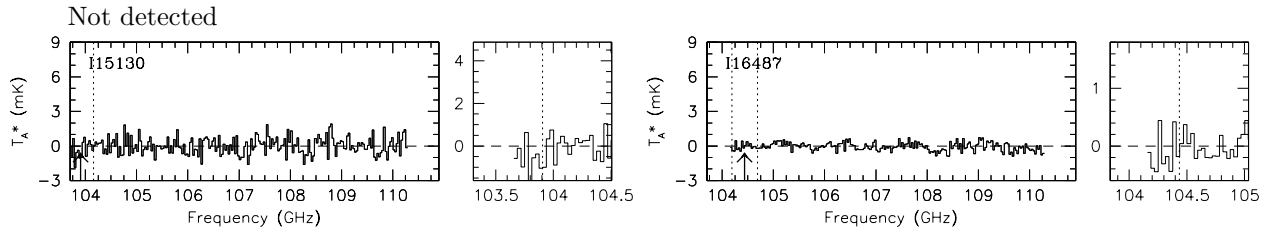

FIG. 3.— (d) The RSR spectra of 2 ULIRGs which were not detected in our study. The dotted lines in the full-band spectra indicate the 1 GHz width ($\sim$ 2600 km s^{-1}) around the inferred CO frequency the optical velocity. The y-axis in the zoom-in spectrum corresponds to -3σ to 5σ as presented in Table 1.

range measured by Solomon et al. (1997) is shown in Figure 7. This plot nicely shows that nearly all of the ULIRGs in our sample are in the lower half of the CO luminosity bins. Probing deeper into the lower CO luminosity objects, we find a broader range of L_{FIR}/L_{CO} ratio for the ULIRG population, including the discovery of a handful of ULIRGs with extremely large L_{FIR}/L_{CO} ratios ($> 250\ L_\odot/L_l$). This newly identified population is discussed further in § 5.1.

4.3. *CO Luminosity and Molecular Gas Mass*

The CO line luminosity, $L'_{\rm CO}$, is calculated as

$$L'_{\rm CO} = 3.25{\times}10^7 I_{\rm CO} \nu_{obs}^{-2} D_L^2\ (1{+}z)^{-3}\ K\ km\ s^{-1}\ pc^2 \quad (2)$$

where $I_{\rm CO}$ is the velocity integrated CO intensity in Jy km s^{-1}, D_L is the luminosity distance in Mpc, ν_{obs} is the observed frequency in GHz, and z is the redshift of the object (Solomon et al. 1992). We used the redshift determined using the CO line to calculate D_L. For the undetected sources, L'_{CO} upper limits are computed using the upper limits of $I_{\rm CO}$ in Table 2 and their optical redshifts. Derived CO luminosities are listed in Table 3.

The CO luminosity of our sample varies by more than a factor of 10, ranging 1.2 – 15.3$\times10^9$ K km s^{-1} pc^2. Adopting the H_2-to-CO conversion factor for starburst systems ($M_{gas}/L'_{\rm CO} \approx 0.8\ M_\odot$ [K km s^{-1} pc^2]$^{-1}$; Downes & Solomon 1998), $L'_{\rm CO}$ of our sample corresponds to 1 – 12$\times10^9$ $M_\odot$ of H_2, which is comparable to normal to gas-rich spiral galaxies (Gao & Solomon 2004b). The median $L'_{\rm CO}$ of our sample, $6 - -7 \times 10^9$ K km s^{-1} pc^2, is about three times as large as the L^* value of the local CO luminosity function (Keres et al. 2003), consistent with a simple model that these ULIRGs are mergers of two massive spiral galaxies.

5. DISCUSSION

5.1. *Non-linear Correlation between L_{FIR} and $L'_{\rm CO}$*

Using the fluxes in the *IRAS* Faint Source Catalog, we have calculated FIR luminosity, L_{FIR} following Lonsdale et al. (1985),

$$L_{FIR} = 4\pi D_L^2\ FIR\ L_\odot \quad (3)$$

D_L is the luminosity distance (see § 4.3) and FIR is the far-infrared flux,

$$FIR = 1.26 \times 10^{-14}\ (2.58 f_{60} + f_{100})\ W\ m^{-2}, \quad (4)$$

where f_{60} and f_{100} are flux densities at 60 and 100 μm in Jy, respectively. Considering the large uncertainty in dust emissivity, we have not applied any color corrections to L_{FIR} in Table 3.

There is a well-known correlation between IR luminosity and CO luminosity for star forming galaxies, presumably driven by the scaling relation between

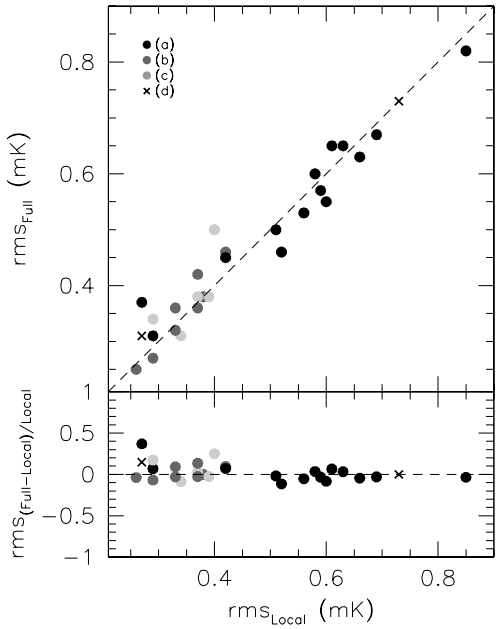

FIG. 4.— Top) A comparison of the full band noise in the coadded RSR spectra to the local rms measured around the CO line (< 2 GHz). Bottom) The percentage differnce in the full band rms and the local rms as a function of the local rms.

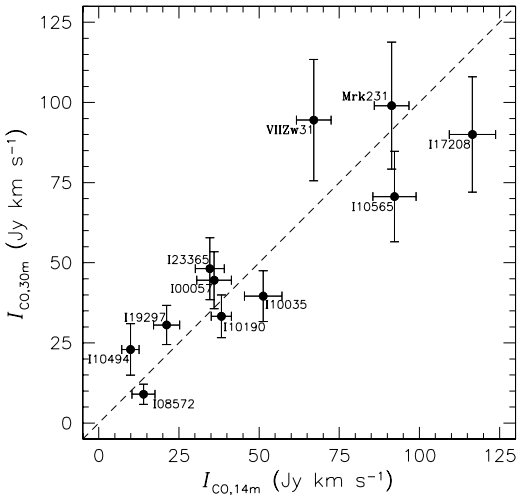

FIG. 5.— Comparisons of $I_{\rm CO}$ from the FCRAO 14m telescope with those measured by the IRAM 30m telescope (Solomon et al. 1997). The antenna gain, G=45 and 4.5 Jy K^{-1} in T'_A and T_{mb} have been adopted for the 14m and 30m telescope, respectively. The 1-σ error bars are shown for both measurements. The dashed line shown is simply a linear relation that corresponds to $I_{\rm CO,30m} = I_{\rm CO,14m}$.

star formation activity and the amount of fuel available (see review by Young & Scoville 1991). This correlation is reproduced in Figure 8, including the 29 new CO measurements of ULIRGs obtained using the RSR system. Galaxies with normal to high star formation rate (Solomon et al. 1997; Gao & Solomon 2004b) and Palomar-Green (PG) QSOs (Alloin et al. 1992; Evans et al. 2001; Scoville et al. 2003) are also shown for comparison. As previously reported (e.g. Sanders et al. 1991; Solomon et al. 1997; Gao & Solomon 2004b), ULIRGs

TABLE 2
^{12}CO $J = 1 \rightarrow 0$ LINE PARAMETERS

Object	rms	$I_{\rm CO}$	$\nu_{\rm CO}$	$W_{\rm CO}$
	mK	K km s^{-1}	GHz	km s^{-1}
I00057	0.51	0.80±0.12	110.36±0.02	347± 91
I05083	0.61	1.49±0.12	109.38±0.01	177± 20
I05189	0.63	0.66±0.16	110.56±0.04	258± 93
I08572	0.34	0.31±0.08	108.86±0.02	290±116
I09111	0.56	0.65±0.12	109.33±0.07	302± 94
I10035	0.59	1.14±0.13	108.30±0.01	320± 63
I10173	0.38	0.26±0.07	109.93±0.01	195± 81
I10190	0.29	0.85±0.07	107.13±0.04	378± 62
I10494	0.26	0.22±0.06	105.58±0.10	213± 77
I10565	0.58	2.05±0.15	110.54±0.00	291± 33
I11095	0.37	0.32±0.10	104.26±0.02	288±138
I12112	0.66	1.43±0.16	107.50±0.03	239± 37
I12540	0.60	2.03±0.12	110.60±0.02	243± 21
I13539	0.29	0.37±0.06	104.01±0.05	223± 53
I14348	0.85	1.06±0.20	106.55±0.09	281± 82
I14394	0.37	0.45±0.10	104.38±0.07	325±113
I15130	0.73	<0.54	.....	.....
I15250	0.39	0.30±0.08	109.27±0.01	238± 96
I15462	0.42	0.25±0.08	104.83±0.05	138± 59
I16487	0.27	< 0.21	.....	.....
I17028	0.40	0.34±0.10	104.30±0.04	281±145
I17132	0.52	1.07±0.10	109.67±0.04	378± 72
I17208	0.69	2.59±0.16	110.54±0.02	294± 28
I18470	0.37	0.32±0.09	106.86±0.01	243±105
I19297	0.27	0.47±0.09	106.20±0.11	308± 96
I20414	0.29	0.22±0.08	106.10±0.11	201± 96
I22491	0.33	0.26±0.06	107.03±0.02	184± 62
I23327	0.33	0.28±0.08	104.06±0.09	220± 94
I23365	0.42	0.77±0.10	108.30±0.03	251± 49

are the most luminous CO emitters in the local universe, with their CO luminosity matching or exceeding those of the most luminous spirals. Unlike most late type galaxies that follow a nearly linear L_{FIR}–$L'_{\rm CO}$ correlation ($L_{FIR}/M_{\rm H_2}$=1-10 $L_\odot/M_\odot$) however, ULIRGs are over-luminous in the far-IR for their CO luminosity ($L_{FIR}/M_{\rm H_2}$=10-100 $L_\odot/M_\odot$), leading to a significant up-turn in the L_{FIR}–$L'_{\rm CO}$ correlation.

Our new survey of 29 ULIRGs has increased the number of ULIRGs with CO measurements to a total of 56. The resulting improvement in the total sample size and statistics provides a better definition of the $L'_{\rm CO}$ distribution as shown in Figure 8. By focusing on the CO-bright and more luminous systems at slightly higher redshifts ($z \lesssim 0.3$), Solomon et al. (1997) established the deviation of ULIRGs from the late type galaxies in the field in the observed L_{FIR}–$L'_{\rm CO}$ correlation. Our study has imporved the statistics particularly on the lower CO luminosity end of the nearby sample at $z \lesssim 0.1$.

PG QSOs as a group have $L_{FIR}/L'_{\rm CO}$ = 67±35 $L_\odot/$[K km s^{-1}], intermediate between ULIRGs (145±79) and late type field galaxies (22±21). As the result of probing the low CO luminosity of the local ULIRG population, ULIRGs and PG QSOs now appear to connect more smoothly in the L_{FIR}–$L'_{\rm CO}$ correlation plot (Fig. 8). The well known correlation between supermassive black holes (SMBHs) and their bulge stellar mass/velocity dispersion (Tremaine et al. 2002; Marconi & Hunt 2003) suggests that the formation/growth of

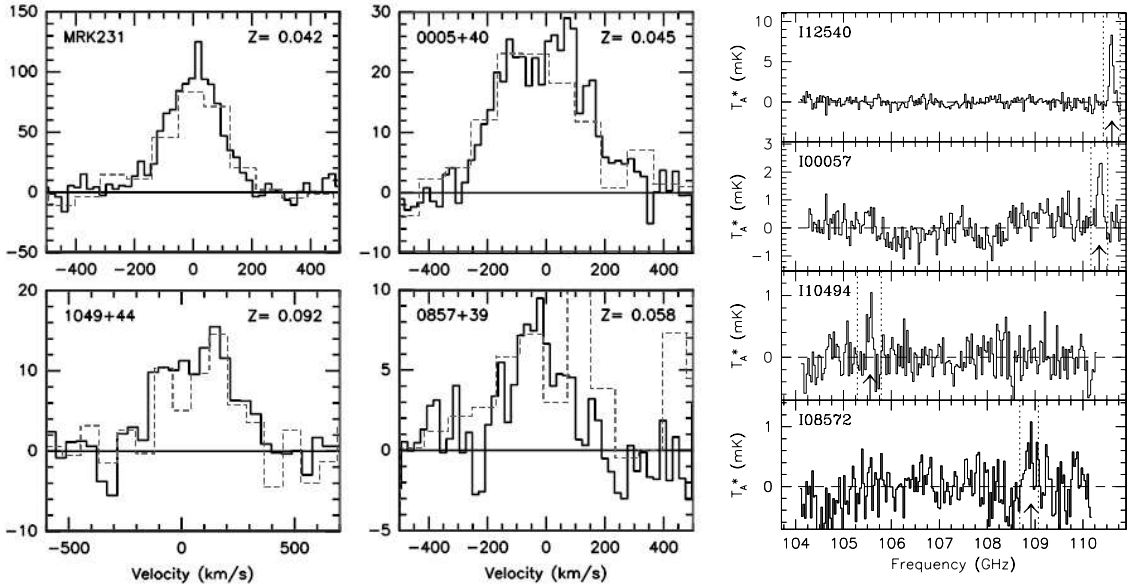

FIG. 6.— Left) Comparisons of the 14m (dashed line) with 30m spectra (solid; Solomon et al. 1997). In the upper row, one example of CO bright (I12540) ULIRG and one with intermediate CO line strength (I00057) are shown. In the bottom, each example show a CO faint object (I10494) and one marginal detection (I08572). The spectra from IRAM 30m is shown in mK in T_{mb} scale as presented in Solomon et al. (1997); Right) The RSR full-band spectra of the four ULIRGs are presented. The y-axis (in mK in T_A^* scale) has been scaled down with the peak CO flux density of each case. The frequency ranges blocked with dotted lines are the regions compared with the study of Solomon et al. (1997) on the left-side. The upper arrow represents the optical redshift as Figure 3.

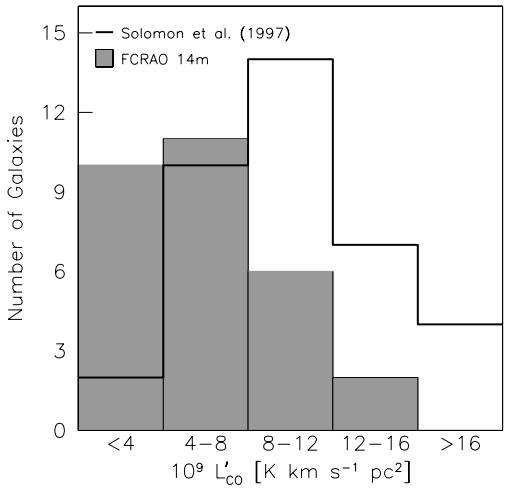

FIG. 7.— Distributions of the sample with different ranges of CO luminosities. The thick line represents 37 low-z ULIRGs ($z < 0.3$) from Solomon et al. (1997) and the shaded area represents 29 local ULIRGs ($z \lesssim 0.1$) from this work.

SMBHs and their stellar hosts may be coupled. Previously, some doubt was expressed on the ULIRG-QSO connection owing to the apparent discrepancy in their $L_{FIR}/L'_{\rm CO}$ ratios (e.g., Yun et al. 2004). However, with a better agreement revealed by our new ULIRG CO survey, this apparent discrepancy (driven by poor statistics and bias in the earlier surveys) is no longer a serious challenge for the ULIRG-to-QSO evolutionary scenario (see 5.2 for further discussion).

A small number of ULIRGs with extreme ratios of $L_{FIR}/L'_{\rm CO} \gtrsim 250\ L_\odot/[{\rm K\ km\ s^{-1}}]$ have been identified by our new ULIRG CO survey (Fig 8 and 9). PDS 456, the most luminous QSO in the local universe at $z = 0.184$, and an ULIRG at $z = 0.059$, I08572 were the only luminous infrared sources previously identified with such an extreme $L_{FIR}/L'_{\rm CO}$ ratio (Yun et al. 2004). Yun et al. (2004) have speculated that these sources may be extremely rare ULIRG-to-QSO transition objects based on the warm IR color and small $L_{FIR}/L'_{\rm CO}$ ratio. Our study has identified seven additional sources, and they are discussed further below, in § 5.4.

5.2. *AGN Activities as the Origin of Large FIR-to-*CO *Luminosity Ratios for ULIRGs*

A number of IR luminous galaxies display characteristics of Seyfert activity in their optical spectrum, indicating that dust heating by AGN activities may make an important contribution to the IR emission. Although the actual frequency is poorly determined (Veilleux 2006), about 5% of IR bright galaxies with $L_{IR} = 10^{10-11} L_\odot$ and up to 50% of the sources with $\log L_{IR} \geq 10^{12.3} L_\odot$ show broad, high excitation lines characteristic of AGN activities (Veilleux et al. 1995; Kim & Sanders 1998; Veilleux et al. 1999; Kewley et al. 2001). An optical spectrum characteristic of Seyfert activity is found in 8 out of 29 galaxies in our sample and 12 out of 29 in the comparison sample of local ULIRGs (Solomon et al. 1997; Gao & Solomon 2004a). Including those with a LINER spectrum (11 and 8), respectively) would increase the fraction of ULIRGs with AGNs.

Given that the bulk of ULIRG luminosity emerges as dust-processed IR emission, optically thin tracers are required to probe the presence of AGN activities with a greater accuracy. Also, since all massive galaxies are expected to host a SMBH (e.g., Tremaine et al. 2002; Marconi & Hunt 2003), demonstrating that AGN activity is the primary source of luminosity is far more impor-

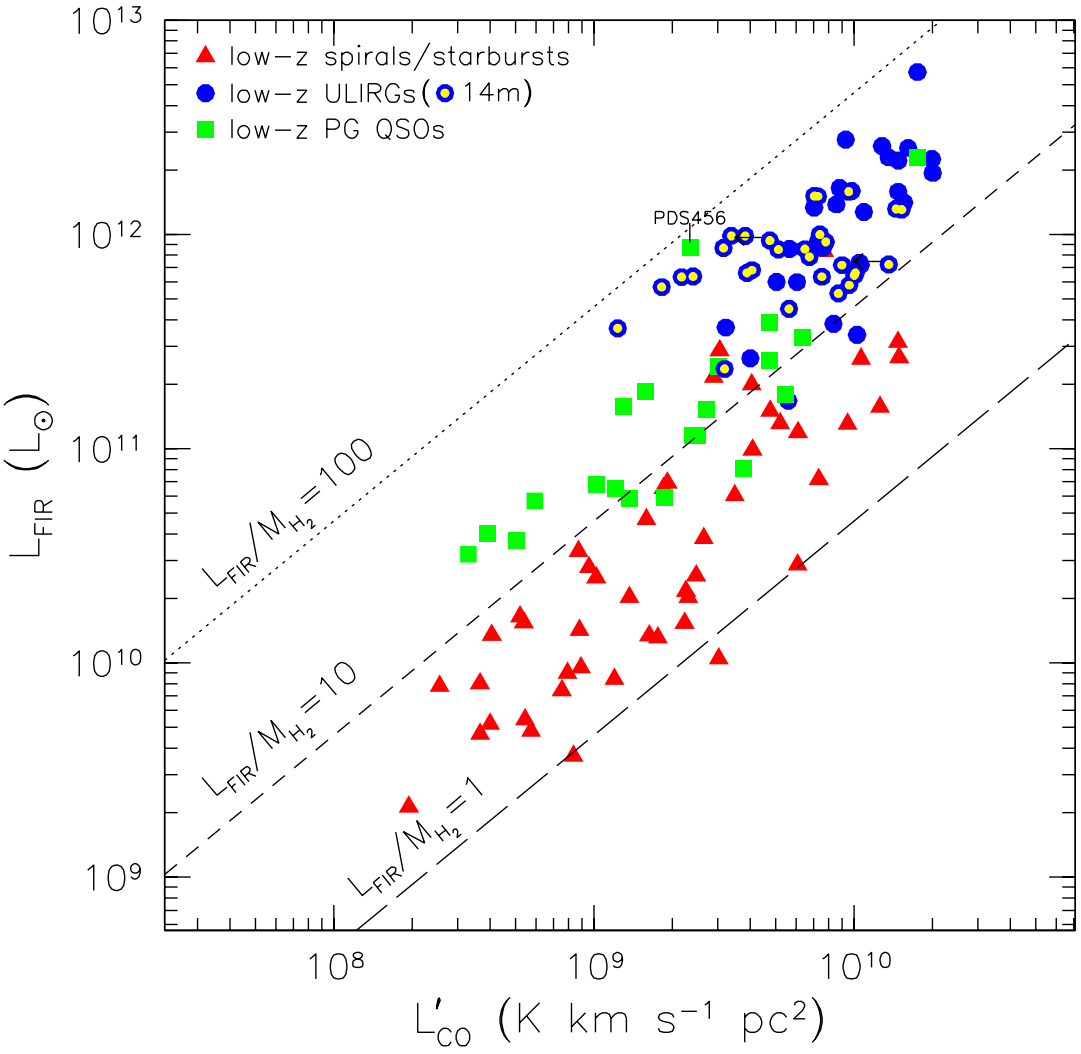

FIG. 8.— L_{FIR} vs. $L'_{\rm CO}$ of low-z galaxies with a range of far infrared luminosity. Spirals and starburst systems from Gao & Solomon (2004b) and Solomon et al. (1997) are shown red triangles, $z \lesssim 0.3$ Paloma- (PG) QSOs from Alloin et al. (1992), Evans et al. (2001), and Scoville et al. (2003) are shown by green squares. ULIRGs by Solomon et al. (1997) are shown in blue circles. The yellow dots with a blue circle around represent the ULIRGs in our sample observed by RSR on the FCRAO 14m telescope. Non-detections are indicated with arrows. Dotted and dashed lines indicate constant ratios of $L_{FIR}/M_{\rm H_2}$ = 1, 10, and 100 using the standard CO-to-H_2 conversion ($M_{\rm H_2}$ [$M_\odot$]= $4.6L'_{\rm CO}$ [K km s^{-1} pc^2]).

tant than establishing the presence of a hidden AGN. For example, Nagar et al. (2003) have reported that a high fraction (∼75%) of ULIRGs with Seyfert or LINER emission lines host compact, non-thermal radio sources among the IRAS 1 Jy ULIRG sample. In contrast, the analysis of the Infrared Space Observatory (ISO) mid-IR spectra (Genzel et al. 1998; Rigopoulou et al. 1999) and IR photometry (e.g. Farrah et al. 2003) have shown that starbursts dominate the luminosity output in most ULIRGs while only 20-30% of ULIRGs are mainly powered by a central AGN in the low-z Universe.

Since the $L_{FIR}/L'_{\rm CO}$ may be an indicator of the efficiency of converting gas mass into luminosity, we explore whether this ratio may offer a useful insight on the nature of the powering sources for the large IR luminosity of ULIRGs. In Figure 10, we plot mid-IR color f_{25}/f_{60}, as a proxy of luminous obscured AGN (de Grijp et al. 1985), against the $L_{FIR}/L'_{\rm CO}$ ratio for the local ULIRGs, PG QSOs, and spirals. These three populations are fairly well separated in this figure with only a small overlap among them. Spirals and ULIRGs have similar mid-IR colors, but ULIRGs are distinguished by their larger $L_{FIR}/L'_{\rm CO}$ ratios. PG QSOs show much warmer mid-IR colors ($f_{25}/f_{60} \geq$0.2), and their $L_{FIR}/L'_{\rm CO}$ ratios are comparable to or somewhat smaller than those of ULIRGs. Only ∼10% of the ULIRGs show mid-IR colors as warm as QSOs. The ULIRGs with Seyfert or LINER spectra are not clearly distinguishable by their mid-IR

TABLE 3
INFRARED AND CO PROPERTIES OF THE SAMPLE

Object	I_{CO} (Jy km/s)	z[a]	L'_{CO} ($10^9 L_l$)[b]	$\frac{f_{25}}{f_{60}}$	f_{60} (Jy)	f_{100} (Jy)	L_{FIR} ($10^{12} L_\odot$)	q
I00057	36.0	0.044	3.18	0.08	4.47	4.30	0.24	2.853
I05083	67.1	0.054	8.72	0.10	5.58	9.62	0.53	2.281
I05189	29.7	0.043	2.41	0.25	13.70	11.40	0.65	2.729
I08572	13.9	0.059	2.18	0.23	7.43	4.59	0.64	3.227
I09111	29.3	0.055	3.88	0.07	7.08	11.10	0.68	2.829
I10035	51.3	0.065	9.59	0.06	4.59	6.24	0.59	2.360
I10173	11.7	0.049	1.24	0.11	5.80	5.47	0.37	2.800
I10190	38.2	0.077	10.03	0.11	3.33	5.57	0.64	2.464
I10494	9.9	0.092	3.82	0.05	3.53	5.41	0.99	2.375
I10565	92.2	0.043	7.53	0.09	12.10	15.10	0.64	2.475
I11095	14.4	0.106	7.40	0.13	3.25	2.53	1.01	2.260
I12112	64.3	0.073	15.25	0.06	8.50	9.98	1.33	2.658
I12540	91.3	0.042	7.27	0.27	31.99	30.29	1.49	2.255
I13539	16.6	0.109	9.00	0.07	1.83	2.73	0.73	2.366
I14348	47.7	0.082	14.53	0.07	6.87	7.07	1.33	2.372
I14394	20.2	0.105	10.14	0.18	1.95	2.39	0.67	1.798
I15130	<24.3	0.109*	<13.61	0.20	1.92	2.30	0.73	2.362
I15250	13.5	0.055	1.83	0.18	7.29	5.91	0.57	2.809
I15462	11.2	0.100	5.13	0.16	2.92	3.00	0.86	2.489
I16487	<9.5	0.104*	<4.75	0.07	2.88	3.07	0.93	2.254
I17028	15.3	0.106	7.79	0.04	2.43	3.91	0.96	2.400
I17132	48.2	0.051	5.63	0.11	5.68	8.04	0.45	2.446
I17208	116.5	0.043	9.54	0.05	31.10	34.90	1.60	2.602
I18470	14.4	0.079	4.06	0.10	4.07	3.43	0.69	2.566
I19297	21.1	0.085	7.05	0.08	7.05	7.72	1.49	2.526
I20414	9.9	0.087	3.38	0.08	4.36	5.25	0.98	2.346
I22491	11.7	0.078	3.15	0.10	5.44	4.45	0.86	3.026
I23327	12.6	0.108	6.74	0.11	2.10	2.81	0.79	2.405
I23365	34.6	0.064	6.48	0.11	7.09	8.36	0.85	2.578

[a]The redshift measured by using the CO line. For non-CO detections, an optically measured z is quoted and indicated with asterisk.
[b]$L_l \equiv$K km s^{-1} pc^2

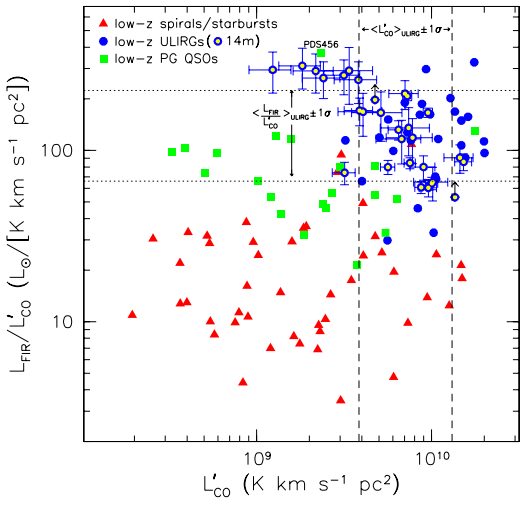

FIG. 9.— L_{FIR}/L'_{CO} vs. L'_{CO}. The same colored symbols are used as Figure 8. The dashed lines and the dotted lines represent $L'_{CO} \pm 1\sigma$ ($8.5 \pm 4.6 \times 10^9$ K km s^{-1} pc^2) and L_{FIR}/L'_{CO} (145 ± 79 $L_\odot$ [K km s^{-1} pc^2]$^{-1}$) of 56 ULIRGs collected in this study. The error bars of our sample reflect the 1σ uncertainties in our CO measurements.

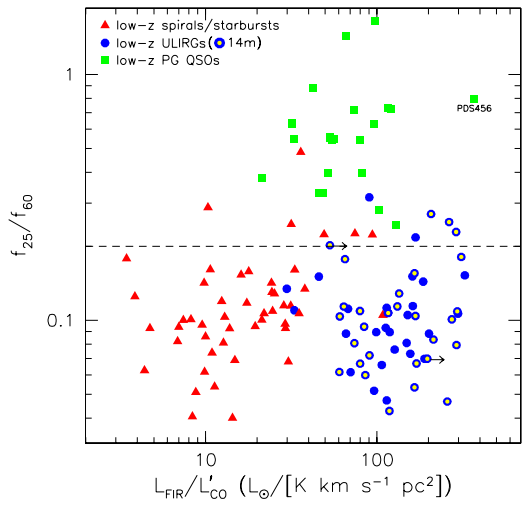

FIG. 10.— Infrared color (f_{25}/f_{60}) vs. L_{FIR}/L'_{CO}. The same colored symbols are used as as Figure 8. The dashed line represents $f_{25}/f_{60} = 0.2$, the borderline of warm and cool ULIRGs.

color. ULIRGs as a group are clearly distinct from PG QSOs in both f_{25}/f_{60} color and in their L_{FIR}/L'_{CO} ratios. These trends imply that the SEDs of most ULIRGs are distinct from those of QSOs and that their mid-IR emission may be indicative of dust heating by a starburst rather than AGN activities. Compared with non-ULIRG starburst systems, however, ULIRGs show a higher efficiency of converting molecular gas into stars as indicated by their high L_{FIR}/L'_{CO} as other studies have previously found.

Another commonly used optically thin indicator of AGN activity is a compact, non-thermal nuclear radio source that produces radio emission in excess of the expected trend from the well-known radio-IR correlation ("radio-excess" with $q \ll 2.1$; see Condon 1992; Yun et al. 2001). For example, the majority of the high redshift QSOs detected both in mm/submm (rest frame far-IR) show radio continuum well in excess of their far-IR luminosity (Yun et al. 2000; Petric et al. 2003; Wang et al. 2007). A quantitative measure of the logarithmic FIR-to-radio flux density ratio, which is known as "q"-parameter, is derived using the following definition,

$$q \equiv log \frac{FIR}{3.75 \times 10^{12} \text{ W m}^{-2}} - log \frac{S_{1.4}}{\text{W m}^{-2} \text{ Hz}^{-1}} \qquad (5)$$

where $S_{1.4}$ is 1.4 GHz radio flux density in W m^{-2} Hz^{-1} (see Condon 1992). Lower q values correspond to higher AGN activity. In Figure 11 we plot q-parameter against L_{FIR}/L'_{CO}. As mentioned earlier, Nagar et al. (2003) have reported a high frequency (∼75%) of compact, non-thermal radio sources among the IRAS 1 Jy ULIRG sample with Seyfert or LINER emission lines. Among the 29 ULIRGs we studied, however, only one object (I14394) shows a clear radio-excess, and the radio-excess ULIRGs are rare among the local ULIRG population in general (see Fig. 11 and Table 4). In the local Universe, only about 1% of the IR-selected galaxies show clear radio-excess (Yun et al. 2001), and only about 10% of optically selected QSOs are radio-loud (Kellermann et al. 1989).

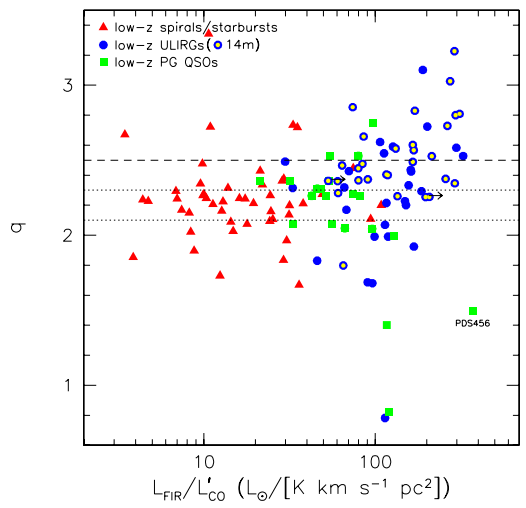

FIG. 11.— A plot of radio-to-FIR luminosity ratio ("q-factor"). The same colored symbols are adopted as Figure 8. The long-dashed and dotted lines represent the mean q and the scatter of Condon (1992)'s sample of spiral galaxies (2.3±0.2).

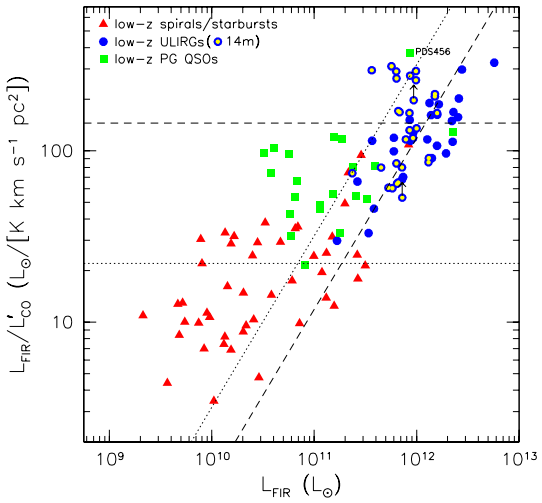

FIG. 12.— $L_{FIR}/L'_{\rm CO}$ vs. FIR luminosity. The dashed lines represent the typical star formation effeiciency (SFE) of the ULIRG sample (145 $L_\odot/L_l \approx 116\ L_\odot/M_\odot$) and $L'_{\rm CO}$ ($8.47 \times 10^9\ L_l$), respectively. Those of the spiral sample (22 $L_\odot/L_l \approx 4$–$5\ L_\odot/M_\odot$, and $3.15 \times 10^9\ L_l$) are indicated with dotted lines (the conversion factors for different populations are given in § 5.4).

Therefore, we can conclude that there is little evidence for a high level of radio AGN activity among the ULIRG population or alternatively can infer a low duty cycle of the radio AGN phase.

5.3. *Merger-induced Starburst Activities as the Origin of Large FIR-to-CO Luminosity Ratios for ULIRGs*

Since there is little direct evidence linking a large FIR-to-CO luminosity ratio and AGN activity, we next explore whether the merger-driven starburst phenomenon can account for the large luminosity ratios observed. In Figure 12, we plot the $L_{FIR}/L'_{\rm CO}$ ratios of ULIRGs and non-ULIRG systems as a function of L_{FIR}. A typical star formation rate of nearby CO-rich spirals ($4\ L_\odot M_\odot^{-1}$) is similar to that of galactic clouds and is generally attributed to recent formation of OB stars in a quiescent disk (e.g. Solomon & Sage 1988). The $L_{FIR}/L'_{\rm CO}$ ratio of 20 $L_\odot M_\odot^{-1}$, shown by a dotted line, is more typical of local starburst galaxies. Yun et al. (2004) and others have noted that PG QSOs display a similar $L_{FIR}/L'_{\rm CO}$ ratio and have proposed a closer physical and evolutionary link with the local starbursts, rather than with the ULIRGs. Most local ULIRGs have a $L_{FIR}/L'_{\rm CO}$ ratio well above the value of non-ULIRG starburst systems, implying that the ULIRG phenomenon not only requires the largest amount of molecular gas found in the most gas-rich systems in the local universe, but it also requires a much more efficient mechanism that converts the gas mass to luminosity. Another potentially important clue to the underlying physical mechanism is that the dispersion in the FIR-to-CO luminosity ratio for the ULIRGs is the largest among the different populations compared. This dispersion may reflect varying evolutionary stages of the ULIRG phase.

A useful insight on the observed $L_{FIR}/L'_{\rm CO}$ ratio (also dubbed "star formation efficiency" Young & Scoville 1991) for the starbursts and ULIRGs is offered by numerical studies of merging disk galaxies. Motivated by a high frequency of morphological peculiarities associated with ULIRGs (Sanders et al. 1988a; Farrah et al. 2001), Mihos & Hernquist (1996) have investigated the response of interstellar medium (ISM) during a merger of two gas-rich spirals and the subsequent secular evolution of the triggered starburst activity. A particularly relevant result from this study is that the compression and concentration of gas (details of which are shown to be highly dependent on the initial conditions) during the course of the merger lead to spikes of elevated starburst activity lasting 5-20 $\times 10^6$ yr (see their Fig. 5). In a more recent simulational study, Matteo et al. (2008) have investigated the enhancement in star formation during galaxy interactions, suggesting that major mergers can increase the star formation efficiency (SFE) by a factor of a few tens compare to that in unperturbed disks which appears to be consistent with what is shown in Figure 12.

We interpret this prediction using our data by drawing lines of constant CO luminosity $L'_{\rm CO}$ (long-dashed lines) in Figure 12. The long dashed line on the right side corresponds to the average CO luminosity of all ULIRGs, and it goes through the upper envelope of the CO luminosity associated with CO-rich spirals in the field. While the long dashed line on the left corresponds to a $L'_{\rm CO}$ 5 times smaller, approximately the L^* value of the local CO luminosity function (10^9 K km s−1 pc^2; Keres et al. 2003).

As one of the CO-rich field galaxies experience a large spike in the massive star formation rate (induced by a galaxy-galaxy collision in the cases of the Mihos & Hernquist study), both L_{FIR} and $L_{FIR}/L'_{\rm CO}$ ratio would increase along the right long-dashed line, reaching the area occupied by the ULIRGs. As the starburst activity fades, the galaxy would climb back down along the same line. Therefore, the apparent broad trend between $L_{FIR}/L'_{\rm CO}$

TABLE 4
AGN Diagnostics for the Extreme L_{FIR}/L'_{CO} ULIRGs

Object	$L_{FIR}/L'_{\rm CO}$	f_{25}/f_{60}	$f_{1.4}$ (mJy)	q
I05189	264	0.25	29	2.73
I08572	290	0.23	4.8	3.22
I10173	295	0.11	11	2.80
I10494	258	0.05	20	2.38
I15250	311	0.18	13	2.81
I20414	292	0.08	25	2.35
I22491	274	0.10	5.8	3.03
I03158	298	0.10	13	2.60
I14070	327	0.07	5.5	2.54

[cf.]The mean ratio of $L_{FIR}/L'_{\rm CO}$ of the ULIRG, the QSO, and the spiral sample collected in this study are 145 (113 excluding 9 extremers in the table), 67, and 22 $L_\odot/L_l$, respectively.

ratio and L_{FIR} seen in Figure 12 can be naturally explained by secular changes in the starburst luminosity (externally triggered or internally by dynamical instabilities such as bars or spiral density waves) to the gas mass ratio.

One may expect the evolutionary trajectory to be somewhat skewed from the right long-dashed line since the starburst activity would consume some of the gas and would possibly remove additional gas through energetic feedback processes (e.g., Heckman et al. 1990; Martin 2005). On the other hand, the resulting higher gas pressure will lead to an increase in CO excitation and line luminosity, partly compensating for the gas mass loss — see the discussions of elevated CO luminosity in nuclear starburst regions by Solomon et al. (1997) and Downes & Solomon (1998). These competing effects should contribute to the tightness in the observed correlation.

5.4. *Extreme $L_{FIR}/L'_{\rm CO}$ Objects and ULIRG Evolution*

An important outcome of our ULIRG CO study is the discovery of a special group of ULIRGs; I10494, I05189, I22491, I08572, I20414, I10173, and I15250 (in the order of increasing $L'_{\rm CO}$). These systems show extreme $L_{FIR}/L'_{\rm CO}$ ratios which ranges from 250 to 310 $L_\odot/L_l$ (Fig. 8), which is greater than the mean of the rest ULIRGs by a factor of two or more. With the standard conversion factor for spiral galaxies, this corresponds to a star formation efficiency of > 50 $L_\odot/M_\odot$ as shown in Figure 8, and potentially > 300 $L_\odot/M_\odot$, adopting the conversion factor for starburst systems (Downes & Solomon 1998). All but one (I15250) had been previously observed in CO by others (Table 1) and five were detected but I20414 although they have not been recognized as a distinct group before. The only other object previously known for such a large $L_{FIR}/L'_{\rm CO}$ ratio is PDS 456, the most luminous QSO in the local universe ($z < 0.3$ Yun et al. 2004). These objects are readily identifiable in Figures 8, 9, and 12 by their extreme $L_{FIR}/L'_{\rm CO}$ ratios, apart from the rest of the ULIRGs. Along with PDS 456, these seven ULIRGs have some of the lowest far-IR luminosity, suggesting that a comparatively larger fraction of their total IR luminosity arises in the mid-IR wavelengths for a given $L_{FIR}/L'_{\rm CO}$. While the extreme $L_{FIR}/L'_{\rm CO}$ of these systems is primarily attributed to low $L'_{\rm CO}$, there are also two objects with a similar $L_{FIR}/L'_{\rm CO}$ but higher $L'_{\rm CO}$ among the sample of Solomon et al. (1997), I03158 and 14070. These are two of the highest luminosity ULIRGs known, with nearly 10 times larger far-IR luminosity than the seven extreme ULIRGs identified in this study such that these may be a different class of objects altogether. However, this luminosity distinction may simply arise from the redshift restriction imposed by the RSR spectrometer. Our sample includes the lowest redshift ULIRGS corresponding to lower luminosities.

As a first step toward understanding the mechanism(s) responsible for their extreme $L_{FIR}/L'_{\rm CO}$ ratio, we examine in detail the known properties of the individual sources, including the two from the Solomon et al. (1997) sample:

- *IRAS 03158+4227.* This $z = 0.134$ ULIRG shows a second core which is much fainter than the one in the center. While the optical morphology is suggestive of a merging event, this object is found near AGN dominated systems in Spoon et al. (2007)'s diagnostic diagram for mid-infrared spectra of IR galaxies, with a relatively small equivalent width of the 6.2 μm PAH emission feature and a weak 9.7 μm silicate strength.

- *IRAS 14070+0525.* This compact $z = 0.264$ ULIRG does not show any obvious signatures of interactions or merging. This system however, has disturbed isophotes (Veilleux et al. 2002) and morphologically classified as a remnant by Dasyra et al. (2006b). Its spectrum shows characteristics of Sy2 (Veilleux et al. 1999).

- *IRAS 05189−2524.* The optical image of this $z = 0.043$ ULIRG suggests that it is in a late stage of a merger with a highly obscured, compact single nucleus (Farrah et al. 2003). It is one of the six ULIRGs in the IRAS Bright Galaxy Sample with the warmest f_{25}/f_{60} color (Sanders et al. 1988a). Presence of both an obscured AGN (Young et al. 1996) and a buried starburst (Dudley 1999) is suggested by a Sy2 spectrum (Veilleux et al. 1995) and an X-ray spectrum characteristic of a Compton thin AGN and a thermal component (Risaliti et al. 2000; Lutz et al. 2004). By modeling the observed SED, Farrah et al. (2003) conclude that $> 30\%$ of the total IR luminosity is contributed by the AGN.

- *IRAS 08572+3915.* This $z = 0.059$ ULIRG shows two cores which are well separated by 6 kpc. Both the stellar nuclei are dominated by Hα emission (Colina, Arribas & Monreal-Ibero 2005). It is also a well-known warm object ($f_{25}/f_{60} = 0.23$) with a strong evidence for an AGN (Soifer et al. 2000; Farrah et al. 2003).

- *IRAS 10173+0828.* This $z = 0.049$ ULIRG looks disky compared to most ULIRGs with a highly asymmetric outer disk. It is a OH megamaser galaxy (OHM), which is thought to be caused by infrared radiation from the surrounding environment (Baan 1985). Most OHMs are known to be warm (U)LIRGs (Chen, Shan, & Gao 2007)

although this system is not a particularly warm ULIRG among the sample with $f_{25}/f_{60} \approx 0.11$.

- *IRAS 10494+4424.* This $z = 0.092$ ULIRG presents two spikes to the north-northwest which (Veilleux et al. 2002) suggest tidal origin. In their SPITZER spectroscopic study, Imanishi et al. (2007) find no signature of a buried AGN in this system, which is consistent with the SED study by Farrah et al. (2003). The upper limit of the AGN contribution to the total IR flux estimated by Farrah et al. (2003) is less than ∼13%.

- *IRAS 15250+3609.* This $z = 0.055$ ULIRG shows a ring-like structure around a spheroid in the center (Scoville et al. 2000) with a much dimmer nucleus 0.7 arcsec away from the center (Farrah et al. 2003). Lutz et al. (1999) have classified it as a starburst/LINER based on its mid-IR spectrum. However, in Farrah et al. (2003)'s SED study, this object has been found with one of the largest AGN contribution ($L_{\rm AGN}/L_{IR} \gtrsim 0.6$) among the sample.

- *IRAS 20414−1651.* This $z = 0.087$ ULIRG was observed in CO by Mirabel et al. (1990) but not detected. It shows a main nucleus with highly elongated isophotes (Veilleux et al. 2002). Murphy et al. (1996) find a double core in the optical which appears to be one system in the infrared. Farrah et al. (2003) find its AGN contribution to the total IR luminosity of ∼ 13%, below the mean of their sample (23%). However, Dasyra et al. (2006b) find a black hole mass of $\gtrsim 10^8\ M_\odot$ (larger than that of I05189 by a factor of ≈ 3.5) based on the bulge dispersion relation (Tremaine et al. 2002).

- *IRAS 22491−1808.* This $z = 0.078$ ULIRG is a close (2.2 kpc) pair with two tidal tails (Veilleux et al. 2002). Cui et al. (2001) have proposed a multiple merger origin for this system, which is also supported by its mid-IR spectrum (Lutz et al. 1999). However, this ULIRG is one of the few objects with the largest AGN contribution ($L_{\rm AGN}/L_{IR} \gtrsim 0.7$) in the sample of Farrah et al. (2003)'s SED study along with I15250.

Based on their high $L_{FIR}/L'_{\rm CO}$ and evidence for AGNs (except I03158 which has not been well studied, and I10494 with the lowest $L_{FIR}/L'_{\rm CO}$), we speculate that these ULIRGs are currently consuming enormous amounts of molecular gas to feed the central black holes, and are likely to become QSOs. The rarity of PDS 456-like QSO however, suggests that the timescale of forming classical quasars in this way is relatively short compared to the timescale of growth of an AGN in a ULIRG phase.

The interconnection between ULIRGs and QSOs has been suggested by Sanders et al. (1988a, b) who have demonstrated the similarity between the SEDs of warm ULIRGs ($f_{25}/f_{60} > 0.2$) and those of QSOs. Warm ULIRGs also morphologically resemble QSOs with a more prominent spheroid, weaker tidal features, and brighter nuclei compared to their cooler counterparts (Veilleux 2006). These observations suggest that cool, starbursting ULIRGs may go through an AGN-like warm ULIRG phase and eventually become optically selected QSOs once the burst of star formation decays and the nucleus sheds its obscuring dust (Sanders et al. 1988a; Yun et al. 2004; Veilleux 2006; Dasyra et al. 2006a).

The transition from a ULIRG phase to a QSO phase can be driven by rapid conversion of gas into stars and/or a subsequent growth of a supermassive black hole (Yun et al. 2004). Due to rapid consumption of gas, transition objects are expected to deviate from the standard ULIRG L_{FIR}-$L'_{\rm CO}$ correlation in the way that results in a larger L_{FIR} for a given molecular gas mass compared to most ULIRGs. There are only a few such ULIRGs that have been found in previous CO studies which are biased to luminous ULIRGs and one QSO, PDS 456 (Yun et al. 2004). In our study however, we find four additional ULIRGs with PDS 456-like $L_{FIR}/L'_{\rm CO}$ along with I08572 which already has been known (Gao & Solomon 1999).

6. SUMMARY

We have presented ^{12}CO $J = 1 \rightarrow 0$ observations of 29 ULIRGs at z=0.043-0.11, using the Redshift Search Receiver (RSR). In total 27 systems have been detected including 9 new detections, which has increased the number of local ULIRGs with CO measurement by 15%. The CO line luminosity $L'_{\rm CO}$ of our sample ranges from 1.2 to 15.3 × 10^9 K km s^{-1} pc^2. Adopting the CO-to-H_2 conversion factor for ULIRGs/QSOs ($M_{\rm H_2}$=0.8 $L'_{\rm CO}$ $M_\odot$ [K km s^{-1} pc^2]$^{-1}$), the inferred cold gas mass in H_2 form in those ULIRGs is 1 – 12×10^9 $M_\odot$. We have investigated $L'_{\rm CO}$ of local ULIRGs as function of IR and radio properties.

1. ULIRGs are 10-100 times higher in $L_{FIR}/L'_{\rm CO}$ than spirals/starburst galaxies and form a continuous track with low-z QSOs, consistent with results from previous studies. However as a result of probing deeper in CO faint objects, our survey finds a broader range of $L_{FIR}/L'_{\rm CO}$, resulting in a smoother transition between the ULIRG and QSO populations.

2. ULIRGs are well separated in f_{25}/f_{60} vs. $L_{FIR}/L'_{\rm CO}$ space from spirals/starburst systems by much larger $L_{FIR}/L'_{\rm CO}$. They are also distinct from QSOs by their cooler mid-IR color ($f_{25}/f_{60} < 0.2$).

3. The radio excess, q of ULIRGs is not significantly different from those of non-ULIRG populations.

4. Seven ULIRGS with extreme values of $L_{FIR}/L'_{\rm CO} \gtrsim 250$ are identified. These are similar to the luminous quasar PDS 456.

From these, we conclude that the power sources of most local ULIRGs are mainly sporadic starbursts which are likely to be driven by merging events, rather than AGNs. However, we always find some evidence for a powerful central source in those ULIRGs with extreme $L_{FIR}/L'_{\rm CO}$, which may be representative of transition objects to QSOs. These objects are not distinct from most ULIRGs in other properties which might be due to a short timescale of the transition.

We would like to thank the anonymous referee for a detailed review of the manuscript and useful comments

that helped to improve the paper. We are grateful to Mike Brewer, Don Lydon, Kamal Souccar, Gary Wallace, Ron Grosslein, John Wielgus, Vern Fath, and Ronna Erickson for their technical support of Redshift Search Receiver commissioning. This work was supported by NSF grants AST 0096854, AST 0540852, and AST 0704966.

REFERENCES

Alloin, D., Barvainis, R., Gordon, M. A., & Antomucci, R. R. J. 1992, A&A, 265, 429
Baan, W. A. 1985, Nature, 315, 26
Blain, A. W., Smail, I., Ivison, R. J., Kneib, J.-P., Frayer, D. T., 2002, *Physics Reports*, 369, 111
Chen, P. S., Shan, H. G., & Gao, Y. F. 2007, ApJ, 133, 496
Colina, L., Arribas, S., & Monreal-Ibero, S. 2005, ApJ, 621, 725
Combes, F., García-Burillo, S., Braine, J., Schinnerer, E., Walter, F., Colina, L, & Gerin, M. 2006, å, 460, L49
Condon, J. J. 1992, ARA&A, 30, 575
Cui, J., Xia, X.-Y., Deng, Z.-G., Mao, S., Zou, Z.-L. 2001, AJ, 122, 63
Dasyra, K. M., Tacconi, L. J., Davies, R. I., Genzel, R., Lutz, D., Naab, T., Burkert, A., Veilleus, S., & Sanders, D. B. 2006a, ApJ, 638, 745
Dasyra, K. M., Tacconi, L. J., Davies, R. I., Naab, T., Genzel, R., Lutz, D., Sturm, E., Baker, A. J., Veilleux, S., Sanders, D. B., & Burkert, A. 2006b, ApJ, 651, 835
de Grijp, M. H. K., Miley, G. K., Lub, J., & de Jong, T., 1985, Nature, 314, 240
Dinh-V-Trung, Lo, K. Y., Kim, D.-C., Gao, Y., & Gruendl, R. A. 2001, ApJ, 556, 141
Downes, D., & Solomon, P. M. 1998, ApJ, 507, 615
Dudley, C. C. 1999, MNRAS, 307, 553
Erickson, N., Narayanan, G., Goeller, R., Grosslein, R. 2007, in *From Z-Machines to ALMA: (Sub)Millimeter Spectroscopy of Galaxies*, ASP Conference Series, Vol. 375, editors A. J. Baker, J. Glenn, A. I. Harris, M. S. Yun, p.71.
Evans, A. S., Frayer, D. T., Surace, J. A., & Sanders, D. B. 2001, AJ, 121, 1893
Farrah, D., Rowan-Robinson, M., Oliver, S., Serjeant, S., Borne, K., Lawrence, A., Lucas, R. A., Bushouse, H., & Colina, L. 2001, MNRAS, 326, 1333
Farrah, D., Afonso, J., Efstathiou, A., Rowan-Robinson, M., Fox, M, & Clements, D. 2003, MNRAS, 343, 585
Gao, Y., & Solomon, P. M. 1999, ApJ, 512, L99
Gao, Y., & Solomon, P. M. 2004a, ApJS, 152, 63
Gao, Y., & Solomon, P. M. 2004b, ApJ, 606, 271
Genzel, R., Lutz, D., Sturn, E., Egami, E., Kunze, D. et al. 1998, ApJ, 498, 579
Heckman, T. M., Armus, L., Miley, G. K. 1990, ApJS, 74, 833
Huchra, J., Davis, M., Latham, D., & Tonry, J. 1983, ApJS, 52, 89
Imanishi, M., Dudley, C. C., Maiolino, R., Maloney, P. R., Nakagawa, T., & Raisaliti, G. 2007, ApJS, 171, 72
Kellermann, K. I., Sramek, R., Schmidt, M., Shaffer, D. B., Green, R. 1989, AJ, 98, 1195
Keres, D., Yun, M. S., & Young, J. S. 2003, ApJ, 582, 659
Kewley, L. J., Heisler, C. A., Dopita, M. A., Lumsden, S. 2001, ApJS, 132, 37
Kim, D.-C., & Sanders, D. B. 1998, ApJS, 119, 41
Kim, D.-C., Veilleux, S., & Sanders, D. B. 1998, ApJ, 508, 627
LeFloc'h, E., et al. 2005, ApJ, 632, 169
Lonsdale, C. J., Helou, G., Good, J. C., & Rice, W. 1985, Catalogued Galaxies and Quasars Observed in the *IRAS* Survey (Pasadena:JPL)
Lutz, D., Veilleux, S., Genzel, R. 1999, ApJ, 517, L13
Lutz, D., Maiolino R., Spoon, H., & Moorwood, F. 2004, A&A, 418, 465
Marconi, A., & Hunt, L. K. 2003, ApJ, 589, L21
Martin, C. L. 2005, ApJ, 621, 227
Matteo, P. D., Combes, F., Melchior, A. L., & Semelin, B. 2008, ASP Conference Series, Vol. 390, edited by J. H. Knapen, T. J. Mahoney, and A. Vazdekis, p. 178
Mihos, J. C., & Hernquist, L. 1996, ApJ, 464, 641
Mirabel, I. F., Booth, R.S., Garay, G., Johansson, L E. B., & Sanders, D. B. 1990, A&A, 236, 327
Moshir, M., et al. 1990, IRAS Faint Source Catalogue, Ver. 2.0 (Greenbelt: NASA)
Murphy, T. W., Armus, L., Matthews, K., Soifter, B. T., Mazzarella, J. M., Shupe, D. L., Strauss, M. A., Neugebauer, G. 1996, AJ, 111, 1025
Murphy, T. W., Jr., Soifer, B. T., Matthews, K., Armus, L., Kiger, J. R. 2001, AJ, 121, 97
Nagar, N. M., Wilson, A. S., Falcke, H., Veilleux, S., & Maiolino, R. 2003, A&A, 409, 115
Narayan, D., Groppi, C. E., Kulesa, C. A., Walker, C. K. 2005, ApJ, 630, 269
Petric, A. O., Carilli, C. L., Bertoldi, F., Fan, X., Cox, P., Strauss, M. A., Omont, A., & Schneider, D. P. 2003, AJ, 126, 15
Riechers, D. A., et al. 2006, ApJ, 650, 604
Rigopoulou, D., Spoon, H. W. W., Genzel, R., Lutz, D., Moorwood, A. F. M., & Tran, Q. D. 1999, AJ, 118, 2625
Risaliti, G., Gilli, R., Maiolino, R., & Salvati, M. 2000, A&A, 357, 13
Sanders, D. B., Soifer, B. T., Elias, J. H., B.F. Madore, Matthews, K., Neugebauer, G., & Scoville, N. Z. 1988a, ApJ, 325, 74
Sanders, D. B., Soifer, B. T., Elias, J. H., Neugebauer, G., & Matthews, K. 1988b, ApJ, 328, L35
Sanders, D. B., Scoville, N. Z., & Soifer, B. T. 1991, ApJ, 370, 158
Sanders, D. B., & Mirabel, I. F. 1996, ARA&A, 34, 749
Scoville, N. Z., Evans, A. S., Thompson, R., Rieke, M., Hines, D., C., Low, F. J., Dinshaw, N., Surace, J. A., & Armus, L. 2000, AJ, 119, 991
Scoville, N. Z., Frayer, D. T., Schinnerer, E., & Christopher, M. 2003, ApJ, 585, L105
Soifer, B. T., Neugebauer, G., Matthews, K., Egami, E., Becklin, E. E., Weinberger, A. J., Ressler, M., Werner, M. W., Evans, A. S., Scoville, N. Z., Surace, J. A., & Condon, J. J. 2000, AJ, 119, 509
Solomon, P. M., & Sage, L. J. 1988, ApJ, 334, 613
Solomon, P. M., Downes, D., & Radford, S. J. E. 1992, ApJ, 387, L55
Solomon, P. M., Downes, D., Radford, S. J. E., & Barrett, J. W. 1997, ApJ, 478, 144
Solomon, P. M., & vanden Bout, P. A. 2005, ARA&A, 43, 175
Spergel, D. N., et al. 2003, ApJS, 148, 175
Spoon, H. W. W., Marshall, J. A., Houck, J. R., Elitzur, M., Hao, L, Armus, L., Brandl, B. R., & Charmandaris, V. 2007, ApJ, 654, L49
Strauss, M. A., Huchra, J. P., Davis, M., Yahil, A., Fisher, K. B., & Tonry, J. 1992, ApJS, 83, 29
Tremaine, S., Gebhardt, K., Bender, R., Bower, G., Dressler, A. et al. 2002, ApJ, 574, 740
Veilleux, S., Kim, D.-C., Sanders, D. B., et al. 1995, ApJS, 98, 171
Veilleux, S., Kim, D.-C., Sanders, D. B. 1999, ApJ, 522, 113
Veilleux, S. Kim, D.-C., & Sanders, D. B. 2002, ApJS, 143, 315
Veilleux, S. 2006, NewAR, 50, 701
Wang, R., Carilli, C. L., Beelen, A., Bertoldi, F., Fan, X., et al. 2007, AJ, 134, 617
Yao, L., Seaquist, E. R., Kuno, N., Dunne, L. 2003, ApJ, 588, 771
Young, J. S., & Scoville, N. Z. 1991, ARA&A, 29, 581
Young, J. S., Xie, S., Tacconi, L., Knezek, P., Viscuso, P. et al. 1995, ApJS, 98, 219
Young, S., Hough, J. H., Efstathiou, A., Wills, B. J., Bailey, J. A., Ward, M. J., & Axon, D. J. 1996, MNRAS, 281, 1206
Yun, M. S., Carilli, C. L., Kawabe, r., Tutui, Y., Kohno, K., Ohta, K. 2000, ApJ, 528, 171
Yun, M. S., Reddy, N. A., Condon, J. J. 2002, ApJ, 554, 803
Yun, M. S., Reddy, N. A., Scoville, N. Z., Robson, E. I., & Tilanus, R. P. J. 2004, ApJ, 601, 723